SECOND EUROPEAN CONFERENCE ON EARTHQUAKE ENGINEERING
AND SEISMOLOGY, ISTANBUL AUG. 25-29, 2014

COLLAPSE POTENTIAL UNDER AFTERSHOCKS TAKING INTO ACCOUNT POST-MAINSHOCK PERMANENT DRIFTS

Jorge RUIZ-GARCIA[1] and Julio D. AGUILAR[2]

ABSTRACT

This paper introduces and evaluates a methodology for the aftershock seismic assessment of buildings taking explicitly into account residual drift demands after the mainshock (i.e., post-mainshock residual drifts, $RIDR_o$). The methodology is applied to a testbed four-story steel moment resisting building designed with modern seismic design provisions when subjected to a set of near-fault mainshock-aftershock seismic sequences that induce five levels of $RIDR_o$. The effect of additional sources of stiffness and strength (e.g. interior gravity frames and slab contribution) and the polarity of the aftershocks is examined in this study. Results of this investigation show that the collapse potential under aftershocks strongly depends on modelling approach (i.e., the aftershock collapse potential is modified when additional sources of lateral stiffness and strength are included in the analytical model). Furthermore, it is demonstrated that the aftershock capacity associated to demolition (i.e., the aftershock collapse capacity associated to a residual interstory drift that lead to an imminent demolition) is lower than that of the aftershock collapse capacity, which mean that this parameter should be a better measure of the building residual capacity against aftershocks.

INTRODUCTION

Recently, there has been an increasing interest in the earthquake engineering community for evaluating the performance of structures under aftershocks. Particularly, several researchers have proposed methodologies to evaluate the post-mainshock residual capacity of a given structure (e.g., a building) to sustain aftershocks (e.g. Luco et al., 2004) and the aftershock fragility of post-mainshock damaged structures (i.e., the probability that a already-damaged structure due to a mainshock increases its state of damage conditioned in the ground motion intensity measure of the aftershock) (e.g., Ryu et al., 2011; Raghunandan et al., 2012). These methodologies require inducing an initial damage state (e.g., severe) to a case-study building and, later, subject the already-damaged building to a set of aftershocks. The initial damage states are related to certain amplitude of roof drift induced by the mainshock earthquake ground motion. However, it should be noted that the definition of a global damage state in a post-mainshock damaged structure involves a certain degree of uncertainty, which has not been included in the methodologies previously proposed.

Unlike maximum interstory drift ratio or roof drift ratio, in-situ residual (permanent) displacements (or lateral residual drift) are a measurable seismic demand after the mainshock, which can be determined using, for example, robotic theodolites (Psimoulis and Stiros 2007) during post-mainshock field reconnaissance. It is believed that an alternative approach for structural seismic

[1] Professor, Universidad Michoacana de San Nicolás de Hidalgo, Morelia, jruizgar@stanfordalumni.org
[2] Research Assistant, Universidad Michoacana de San Nicolás de Hidalgo, Morelia, jdaniel_as@hotmail.com

assessment under aftershocks should be based in the explicit consideration of post-mainshock residual drifts that a structure would experience.

The objective of this work is to present an alternative approach for aftershock seismic assessment taking into account lateral residual drifts triggered after the mainshock (i.e., post-mainshock residual drifts). Following this approach, this paper examines the aftershock collapse potential and the aftershock capacity associated to demolition of a testbed four-story steel building. The influence of including several sources of stiffness and strength in the modeling of the case-study building as well as the effect of aftershock polarity are evaluated and discussed in this paper.

METHODOLOGY

An assessment procedure for evaluating the seismic performance against aftershocks is presented in this study, which takes explicitly into account the amplitude of lateral residual drift demands after the mainshock seismic event. Particularly, the procedure can be applied for computing the collapse potential against aftershocks and the residual post-mainshock capacity. For this purpose, the following steps can be envisioned:

1. Develop a suitable analytical model of a case-study building, in its undamaged condition.
2. Select a suitable set of mainshock-aftershock seismic sequences representative of the seismic hazard of the site of interest.
3. For a given mainshock-aftershock seismic sequence, select different levels of residual drift (e.g. maximum residual inter-story drift ratio or roof residual drift ratio) after the mainshock earthquake excitation (i.e., target post-mainshock residual drifts).
4. Scale, in amplitude, each as-recorded mainshock earthquake ground motion in such manner that the building model reaches the selected target post-mainshock residual drift under the scaled mainshock ground motion.
5. Develop IDA of the leaned building (i.e., in its post-mainshock state) under the corresponding aftershock ground motion record up to collapse. Collapse is reached when the building exhibits dynamic instability due to large lateral drift demands.

In this study, the spectral acceleration corresponding to the first mode period of the building, $S_a(T_1)$, was selected as ground motion intensity measure of both the mainshock and aftershock earthquake ground motion. Therefore, the seismic intensity associated to collapse under the aftershock is designated as $S_{a,A}$ (i.e., the aftershock collapse capacity). Similarly, the mainshock collapse capacity can be computed from performing IDA of the original (i.e., undamaged) case-study building, which is named $S_{a,M}$. With both collapse capacities, it is possible to estimate the residual capacity index to sustain aftershocks as follows:

$$\kappa = \frac{S_{a,A}}{S_{a,M}} \tag{1}$$

As it can be anticipated, the residual capacity index will be a function of the level of post-mainshock residual drift demand.

It should be noted that the building could experience excessive lateral residual drifts before it reaches its aftershock collapse capacity, which would lead to its *demolition*. Therefore, it is interesting to evaluate the aftershock capacity associated to demolition, $S_{a,D}$. (i.e., the seismic intensity associated to a lateral residual drift demand that drive the building to its demolition). For evaluating the aforementioned methodology, a testbed four-story steel building is chosen as a case-study.

CASE-STUDY BUILDING CONSIDERED IN THIS STUDY

Description

For illustrating the proposed aftershock assessment procedure, a four-story steel building was selected in this investigation. The building under consideration was specifically designed to investigate the collapse prediction of modern steel structures located in sites of high seismicity (Lignos, 2008; Lignos and Krawinkler, 2011), and served as a prototype for developing one-eight scale models tested in a

shake-table facility. Fig. 1 shows the plan view and elevation of the prototype building. The prototype was designed following the IBC–2003 and AISC–341-05 standards in the U.S. As usual in American design practice, the building includes perimeter moment-resisting frames along with interior gravity frames. Particularly, as recommended for modern steel construction, the beams where designed with reduced beam sections. Comprehensive information about the design process of the prototype building can be found in (Lignos, 2008).

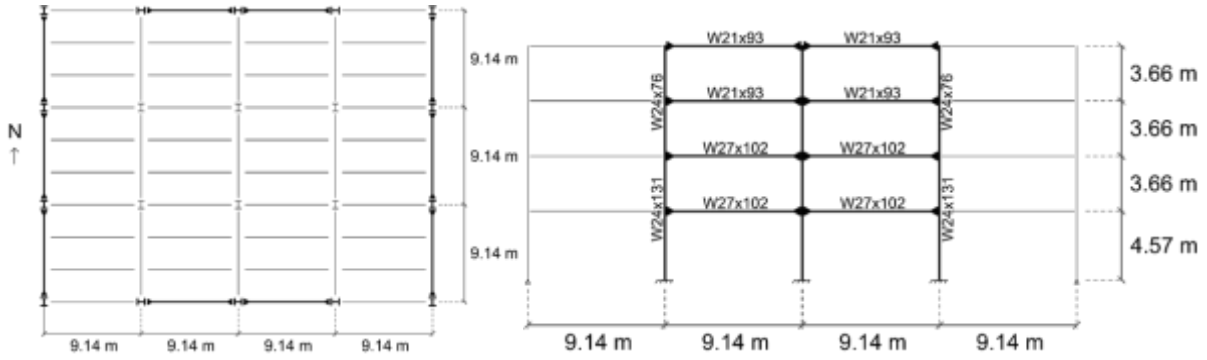

(a) (b)

Figure 1. Case-study steel framed-building considered in this study: a) Plan view, b) East-West elevation.

Modeling

The testbed building was modeled using the computational platform *OpenSees* (2014). Only half of the building was modeled due to its symmetry in the building's plan. Two analytical models were prepared for this investigation. The first model, denoted as M1, only includes the exterior moment-resisting frame, while a second model, denoted as M2, incorporates several additional sources of lateral stiffness and strength. In the M1 model, the exterior two-way frame in the East-West direction was modeled as two-dimensional (2D) centerline model with an additional fictitious column, which is a common modeling strategy in the U.S. The fictitious column carries the vertical (gravity) loading from the rest of building (i.e., vertical loading carried by the interior gravity columns) and is attached to the exterior frame model through rigid frame elements to experience the same lateral deformation at each floor. However, the fictitious column does not provide the additional lateral stiffness from the interior gravity columns. Unlike building model M1, building model M2 includes explicitly one interior gravity frame.

For both analytical models, beams and columns were modeled as two-dimensional, prismatic beam elements composed of an elastic beam element with semi-rigid rotational springs at the ends that concentrates their inelastic behavior (i.e., moment-rotation hysteretic behavior) according to what has been discussed in (Zareian and Medina, 2009). The hysteretic behavior in the rotational springs accounts for structural cyclic degradation (i.e., strength and stiffness degradation) using the modified Ibarra-Krawinkler (MIK) model, which is described in detail in (Lignos, 2008; Lignos and Krawinkler, 2011a) and implemented in *OpenSees* platform (2014). The parameters of the backbone curve in the MIK model for beams were obtained from those proposed in (Lignos, 2008; Lignos and Krawinkler, 2011a) based on calibration using experimental results of the small-scale connections employed in the one-eight scale specimen. In addition, panel zone flexibility was taken into account in each building model following the modeling technique proposed in (ATC, 2010). It should be noted that the slab contribution was not taken into account in the beam's stiffness and strength for building model M1, which is consistent with the modeling assumptions followed by Lignos and Krawinkler (2011b). However, the contribution of the slab was explicitly included in building model M2 by using a larger beam's moment of inertia and asymmetric moment-rotation hysteretic relationship (i.e., with moment capacity in the positive bending direction 10% greater than that in the negative bending direction).In addition to identical modeling strategies in the exterior moment-resisting frame, model M2 included two additional gravity-frame bays and one interior gravity frame. The interior beams were also modelled taking into account their moment capacity. Before performing nonlinear dynamic

analysis, conventional modal analysis and nonlinear static (pushover) analysis were carried out to obtain the dynamic and mechanical properties of both building models. Fig. 2 shows a comparison of the capacity curve corresponding to building models M1 and M2, while Table 1 reports relevant dynamic and mechanical feature. From the figure, it can clearly be seen that the additional sources of stiffness and strength have significant influence in the capacity curve.

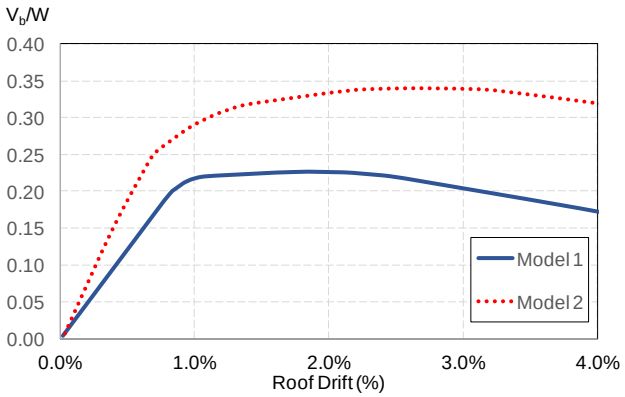

Figure 2. Comparison of capacity curves for building models M1 and M2.

Table 1. Dynamic and mechanical properties of the building models (T_1 is the first-mode period of vibration, Cy is the yield strength coefficient, θy is the roof drift at yielding, and $\Gamma_1\Phi_{1,roof}$ is the normalized modal participation factor).

Building model	T_1 (s)	Cy	θy (%)	$\Gamma_1 \Phi_{1,roof}$
M1	1.28	0.26	0.92	1.29
M2	1.06	0.36	0.88	1.28

Next, nonlinear dynamic time-history analyses were carried out using Newmark constant average acceleration method with time step equal to 0.001s to enhance convergence. Rayleigh damping equal to 3% of critical was assigned to the first and second modes. During the analysis, local P-delta effects were included (i.e., large displacement analysis).

Calibration

Adequate collapse assessment requires analytical models that reassemble the expected seismic behavior of structures. Therefore, the seismic response of building model M1 was calibrated against experimental results obtained in shake-table testing. The testbed frame, designated as Frame 1, was subjected to the earthquake ground motion recorded at Canoga Park station during the 1994 Northridge earthquake (Lignos, 2008; Lignos and Krawinkler, 2011). The record was scaled, in amplitude, to reach four different intensity levels associated to the service-level earthquake (SLE), design-level earthquake (DLE), maximum considered earthquake (MCE) and collapse-level earthquake (CLE). For the shaking-table test, the earthquake record was sequentially scaled to reach each of the intensity levels. Therefore, experimental results were gathered from the NEES repository website and compared with the analytical prediction employing building model M1 previously described. Fig. 3 presents a comparison of the experimental and analytical maximum (transient) and residual (permanent) interstory drift profiles for the case-study frame. It can be seen that analytical prediction is in good agreement with the experimental results for both peak and residual interstory drifts, even under the MCE intensity level.

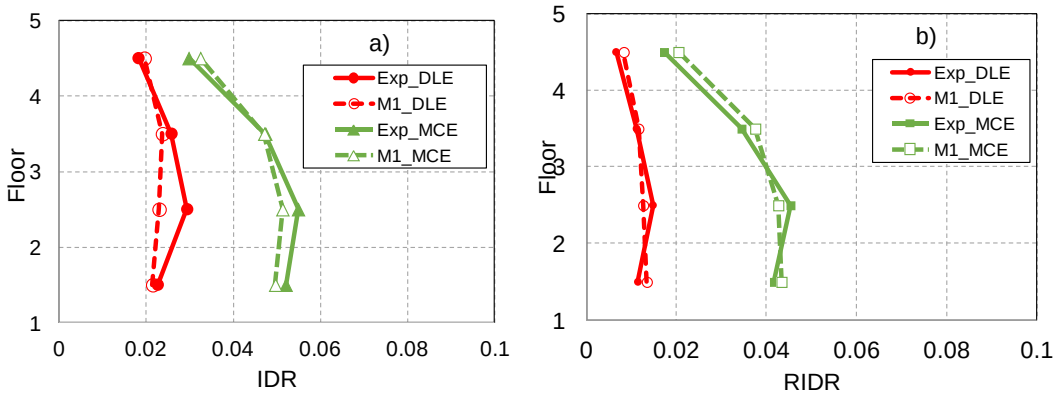

Figure 3. Comparison of experimental (Frame 1) and analytical, obtained from building model M1, peak and residual interstory drift profiles.

AFTERSHOCK COLLAPSE ASSESMENT UNDER INDIVIDUAL SEISMIC SEQUENCES

In this investigation, relevant results are obtained from the seismic response of the building models when subjected to a set of 13 Near Fault-Near Fault seismic sequences gathered during the 1994 Northridge earthquakes, which include those recorded at Sylmar Converter Station and Tarzana Station. A detailed list of the ground motion features of the seismic sequences considered in this study can be found in Ruiz-García and Negrete-Manriquez (2011).

Target maximum residual drift demands

The methodology introduced in this paper relies on the definition of relevant post-mainshock residual drifts, which could be either the maximum residual interstory drift or the roof residual drift. For instance, a recent field investigation carried out in reinforced concrete buildings built in Japan highlighted that a residual inter-story drift of about 0.5% is perceptible for building occupants and a residual inter-story drift of about 1.0% could cause human discomfort (McCormick et al., 2008). Iwata et al. (2006) highlighted that the cost of repair leaned steel buildings linearly increased as the maximum and roof residual drift increased. Based on their study, the authors suggested that steel buildings should be limited to maximum residual interstory and roof residual drift limits of about 1.4% and 0.9%, respectively, to satisfy a reparability limit state that meet both technical and economical constraints. Additionally, FEMA P-58 (2012) recommendations suggest that there is a certainty that a building experiencing a maximum residual interstory drift of 2% will not be repaired. Based on the aforementioned recommendations, it was decided to set five target $RIDR_o$ in this study ($RIDR_o$ =0.1%, 0.5%, 1.0%, 1.4%, and 2.0%). Therefore, each mainshock earthquake ground motion was scaled, in amplitude, in such a manner that each undamaged case-study building reaches $RIDR_o$ after performing nonlinear dynamic analysis.

Response of building models

Initially, IDA is carried out until the original (i.e., undamaged) building model reaches its dynamic collapse capacity in order to compute, $S_{a,M}$. For instance, Fig. 4 shows the evolution of maximum, IDR_{max}, and residual, $RIDR_{max}$, interstory drift of both models as the intensity of the Sylmar (comp. 288) mainshock ground motion intensity grows up to collapse (noted with a black circle). IDR_{max} is presented in absolute value, while $RIDR_{max}$ is shown in relative value with respect to the initial position. As it might be anticipated, the M2 building model has greater collapse capacity than the M1 building model due to inclusion of additional sources of overstrength in its modeling. Also, it is interesting to note that the M1 building model develops a re-centering behavior (i.e., it moves back to its initial position after experiencing residual drifts in one direction), unlike the M2 building model. The influence of re-centering behavior on the aftershock collapse capacity is discussed later.

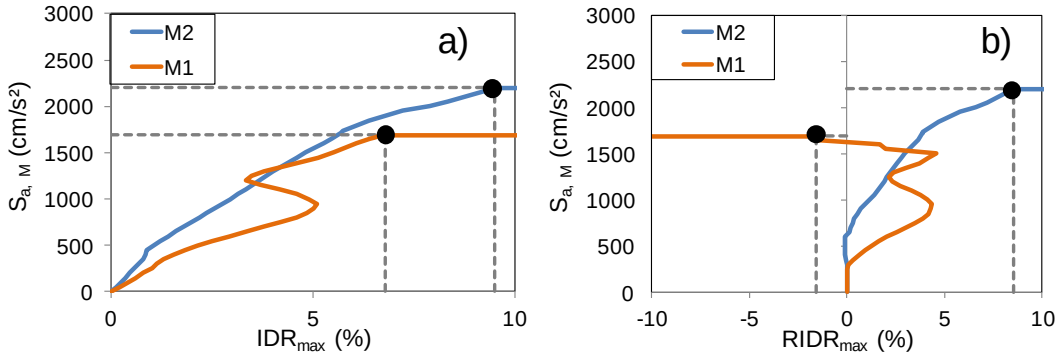

Figure 4. IDA curves to obtain the mainshock collapse capacity of the M2 model under Sylmar (comp. 288) record: a) IDR_{max}, and b) $RIDR_{max}$.

Subsequently, the Sylmar (comp. 288) mainshock acceleration time-history was scaled, in amplitude, in such a manner that both building models reach six levels of $RIDR_o$. After reaching each target residual drift, IDA was applied to each building model under the Sylmar aftershock record to compute its $S_{a,A}$. Fig. 5 shows the aftershock IDA curves for IDR_{max} and $RIDR_{max}$ corresponding to each target $RIDR_o$. It can be seen that the aftershock collapse capacity decreases with respect to the mainshock collapse capacity regardless of the target $RIDR_o$. For example, the aftershock collapse capacity reduces from about 2200 cm/s^2 (2.24g) to 1070 cm/s^2 (1.07g) for target $RIDR_o$ equal to 1.4%, which means a residual capacity index κ around 0.48 (i.e., reduction of 52% in its original collapse capacity). As it may be expected, the aftershock collapse capacity depends on the level of $RIDR_o$. For example, $S_{a,A}$ for a $RIDR_o$ equal to 0.1% reduces from about 1150 cm/s^2 (1.17g) to 1070 cm/s^2 (1.07g) for a $RIDR_o$ equal to 2.0%. In the figure, it is also indicated the $RIDR_{max}$ associated to imminent demolition of the building, which also depends on the $RIDR_o$. From Figure 8b, it can clearly be seen that the intensity capacities associated to demolition, $S_{a,D}$, are smaller than those associated to $S_{a,A}$. This observation suggests that the aftershock capacity of buildings that experience a post-mainshock interstory residual drift should be measured in terms of the remaining capacity to limit the building to sustain a threshold residual interstory drift related to demolition in the event of a strong aftershock rather than the capacity to collapse under the aftershock.

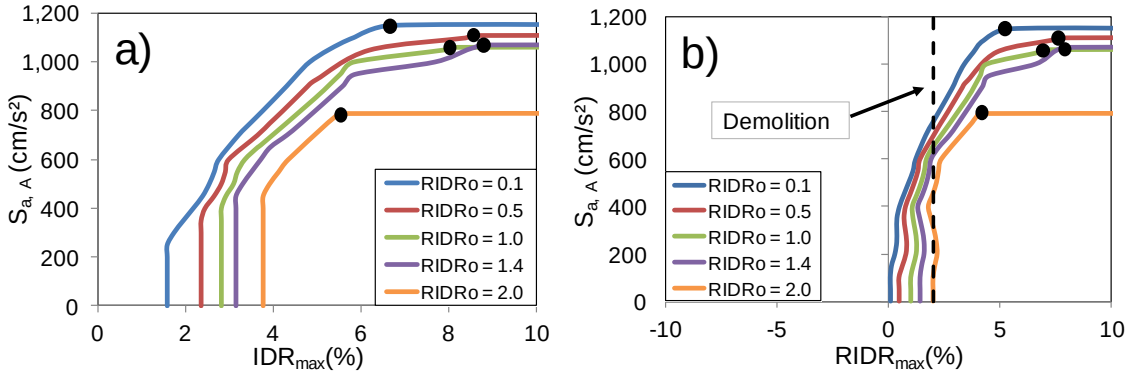

Figure 5. Post-mainshock IDA curves to obtain the aftershock collapse capacity of the M2 building model under Sylmar aftershock record: a) IDR_{max}, and b) $RIDR_{max}$.

Next, Fig. 6 shows a comparison of post-mainshock IDA curves corresponding to both building models for a $RIDR_o$ equal to 1.0%. The $S_{a,A}$ and $S_{a,D}$ are indicated in the figure with black and red circles, respectively. It can be seen that the $S_{a,A}$ and $S_{a,D}$ strongly depend on the modeling approach, since the M2 building model have greater capacities than the M1 building model. Similar observations were found from other levels of $RIDR_o$.

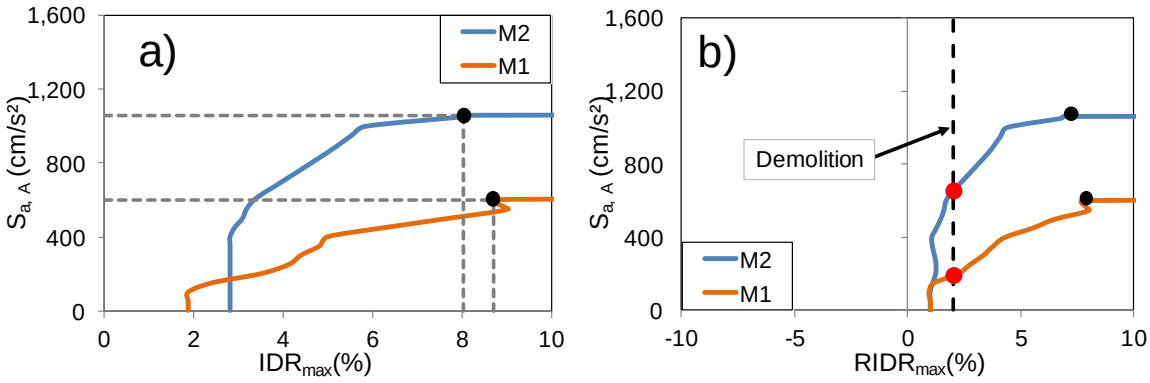

Figure 6. Comparison of post-mainshock IDA curves corresponding to building model M1 and M2 under Sylmar (comp. 288) aftershock record: a) IDR_{max}, and b) $RIDR_{max}$.

It is worth noting that although the aftershock collapse capacity is greater when additional sources of overstrength are included in the M2 building model, the residual capacity index κ is very similar for both building models under this selected earthquake ground motion, as it can be seen in Fig. 7. From the figure, it can also be observed that κ is smaller than one (i.e., the building model has smaller collapse capacity to sustain the aftershock than that under the mainshock) and slightly decreases as the post-mainshock residual drift increases. However, this trend of κ was not always observed under other seismic sequences. For instance, Fig. 8a illustrates the post-mainshock IDA curves corresponding to building model M2 when subjected to the aftershock of sequence JEPG (comp. 022). It can be observed that mainshock collapse capacity is lower than the aftershock collapse capacity, regardless of the level of $RIDR_o$. For this case, the residual capacity index κ becomes greater than one, which means that κ might not be meaningful for measuring the collapse potential against aftershocks. Since the building model has been already carried out to a post-mainshock leaned condition, it would be more meaningful to compare its aftershock collapse capacity for different levels of $RIDR_o$ against its collapse capacity computed from the aftershock earthquake ground motion when $RIDR_o$=0% (i.e., it is assumed that the building model did not experience any post-mainshock residual drift and its original capacity remains intact) as a modified measure of its residual capacity. Therefore, Fig. 8b shows the post-mainshock IDA curves including the IDA curve obtained for the intact M2 building model subjected to the aftershock earthquake ground motion. Now, it can be seen that the aftershock collapse capacity for the intact case is greater than those computed for different levels of RIDRo. This observation suggests redefining the residual capacity index given in Equation 1 as follows: $\kappa^* = S_{a,A} / S_{a,A^*}$, where S_{a,A^*} is the aftershock collapse capacity obtained from the intact building.

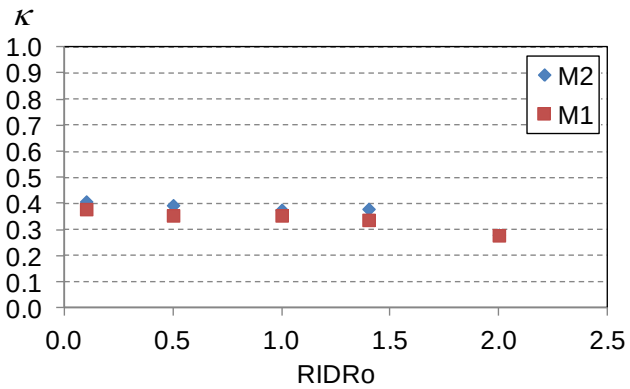

Figure 8. Variation of residual capacity index (Equation 1) with respect to $RIDR_o$ for both building models.

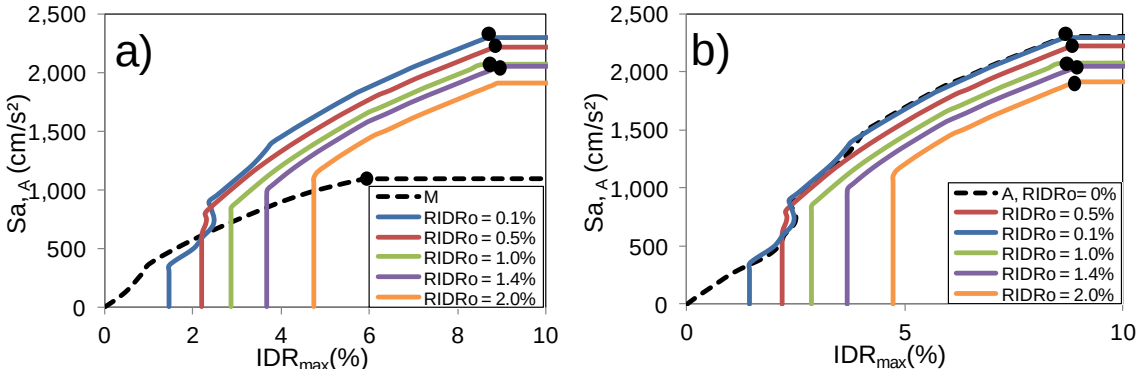

Figure 9. a) comparison of mainshock IDA and post-mainshock IDA curves; b) comparison of post-mainshock IDA curves with $RIDR_o$=0 and post-mainshock.

Re-centering behavior under aftershocks

While developing post-mainshock IDAs under the set of aftershocks, it was noted that the case-study buildings experienced a re-centering mechanism under some aftershocks. That is, the amplitude of initial post-mainshock residual drifts tend to be smaller as the aftershock intensity grows, and the building model exhibits residual drifts in the opposite direction at high aftershock intensity levels. To illustrate this behavior, Fig. 10 shows the third-story time-story drift mainshock-aftershock response of the M2 building model under sequence gathered at Tarzana station (comp. 360), corresponding to $RIDR_o$ equal to 0.1% and 2.0%. It can be seen that the aftershock earthquake ground motion, scaled to reach a $S_{a,A}$ equal to 1000 cm/s^2, tends to move the building model to the opposite direction of the original post-mainshock residual drifts. However, the building model moves back to its straight position when it has already experience a post-mainshock residual drift of 2%, while the building model increases its 0.1% post-mainshock residual drift in the opposite direction. As a result of this re-centering behavior, the aftershock collapse capacity for low $RIDR_o$ becomes smaller than that for high $RIDR_o$ as shown in Fig. 11.

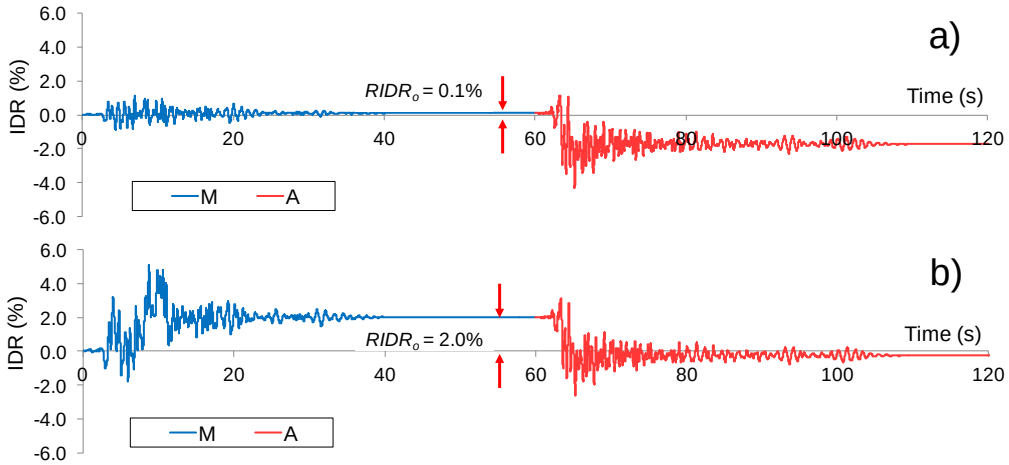

Figure 11. Re-centering behavior observed in third-story drift time-history for two levels of $RIDR_o$: a) 0.1%, and b) 2.0%.

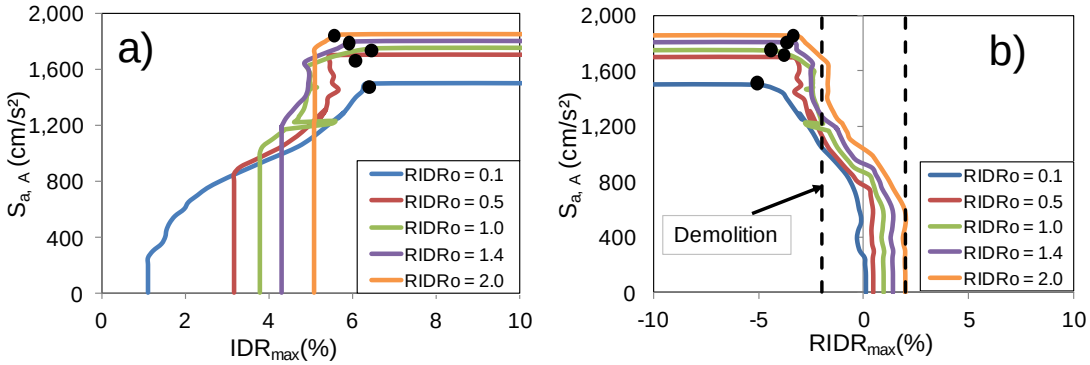

Figure 12. Post-mainshock IDA curves to obtain the aftershock collapse capacity of the M2 model under Sylmar aftershock record: a) IDR$_{max}$, and b) RIDR$_{max}$.

Aftershock polarity

Previous studies have considered that the mainshock-aftershock could have different polarity (Raghunandan et al., 2011) (i.e., it is assumed that mainshock or the aftershock acceleration time-history in a sequence could have the opposite as-recorded). Therefore, to study the effect of polarity on the aftershock collapse potential, the aftershock assessment was repeated for building model M2 assuming that the Sylmar (comp. 288) aftershock could have positive polarity (i.e., as-recorded acceleration time-history), PP, and negative polarity (i.e., opposite direction of the as-recorded acceleration time-history), PN. For instance, Fig. 13 illustrates the first-story time-history drift mainshock-aftershock response assuming a $RIDR_o$ equal to 1.0% and that the aftershock earthquake ground motion was scaled to reach a $S_{a,A}$ equal to 980 cm/s^2. As it might be expected, the post-mainshock residual drift deviates in the opposite direction when PN is assumed and, furthermore, it may lead to a re-centering behavior.

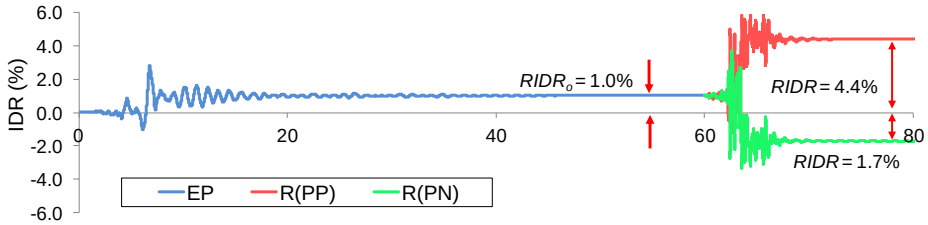

Figure 13. Effect of aftershock polarity in the post-mainshock seismic response of building model M2.

Fig. 14 shows a comparison of post-mainshock IDA curves considering PP and PN polarity for a $RIDR_o$ equal to 1.0%. It can be observed that the polarity of the aftershock ground motion has not only a significant influence on the aftershock collapse capacity (indicated in black circles), but also in the aftershock capacity against demolition (indicated in red circles). Particularly, when the aftershock acts with negative polarity, the building model begin to develop a re-centering behavior at low intensities, and residual drifts ends in the opposite original direction of $RIDR_o$.

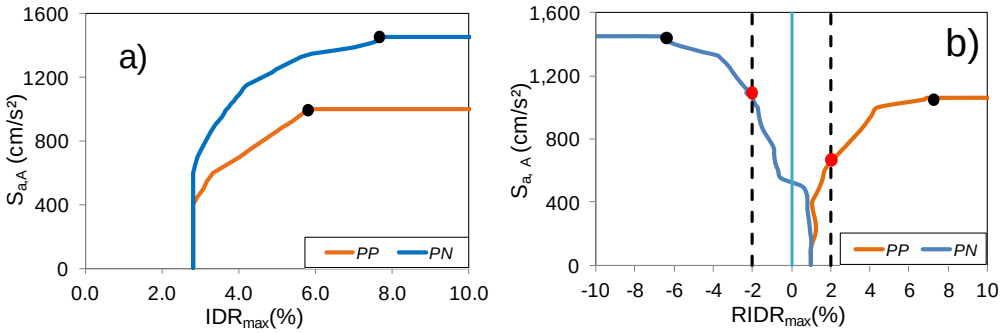

Figure 14. Comparison of post-mainshock IDA curves considering positive and negative polarity of the aftershock: a) IDR$_{max}$, and b) RIDR$_{max}$.

AFTERSHOCK ASSESSMENT UNDER SETS OF SEISMIC SEQUENCES

Following the procedure outlined and illustrated in the previous Sections, a statistical study was conducted to evaluate $S_{a,A}$ and, particularly, the residual capacity to sustain aftershocks of the M1 and M2 building models under the Californian NF-NF sets of seismic sequences. In addition, $S_{a,D}$, is also computed for each sequence and statistically examined.

Fig. 15 shows the evolution of median κ with changes in the $RIDR_o$ for both M1 and M2 building models taking into account positive polarity of the aftershocks. As illustrated in Fig. 16a, it can be seen that the median $S_{a,A}$ of building model M1 slightly decreases as the $RIDR_o$ increases (e.g., from 0.55 for $RIDR_o$ equal to 0.1% to 0.44 for $RIDR_o$ equal to 2.0%). Residual capacity indices greater than one were computed in two cases when the building model developed re-centering behavior. As shown in Fig. 15b, similar evolution can be observed for the M2 building model, but its residual collapse capacity is greater than that of model M1 (e.g., from almost 1.00 for $RIDR_o$ equal to 0.1% to 0.84 for $RIDR_o$ equal to 1.4%). Additionally, Fig. 16 shows a similar plot obtained for the case of negative polarity. Main difference with respect to the previous figure arises from the opposite trend of the M1 building model; that is, κ seems to slightly increase as $RIDR_o$ increases.

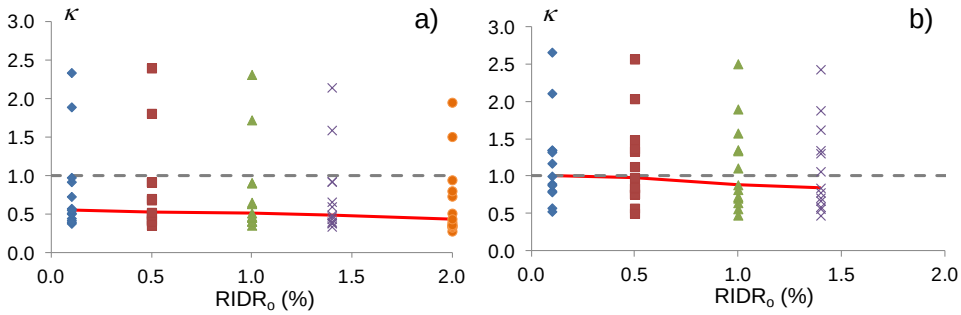

Figure 15. Residual capacity index computed from the NF-NF seismic sequences (positive polarity) for both models considered in this study: a) model M1; b) model M2.

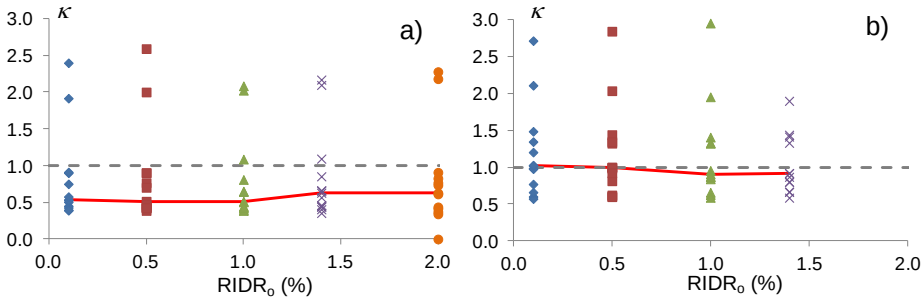

Figure 16. Residual capacity index computed from the NF-NF seismic sequences (negative polarity) for both models considered in this study: a) model M1; b) model M2.

The modified residual capacity index κ^* was also computed as part of this investigation. Fig. 17 shows the evolution of κ^* as $RIDR_o$ increases for both building models when positive polarity is assumed. It can also be seen that κ^* decreases as $RIDR_o$ increases for both building models. For example, κ^* reduces from almost one for $RIDR_o$ equal to 0.1% to 0.93 and 0.78 for $RIDR_o$ equal to 1.4% and 2.0%, respectively, for building model M1. Similarly, κ^* reduces from almost one for $RIDR_o$ equal to 0.1% to 0.91 for $RIDR_o$ equal to 1.4% for building model M1. The building model M1 reaches slightly smaller values of κ^* than building model M2 since the latter model experienced more cases of re-centering behavior, which occurred when κ^* is larger than one. Finally, it should be noted that different median values of κ and κ^* can be obtained when considering a different set of seismic sequences.

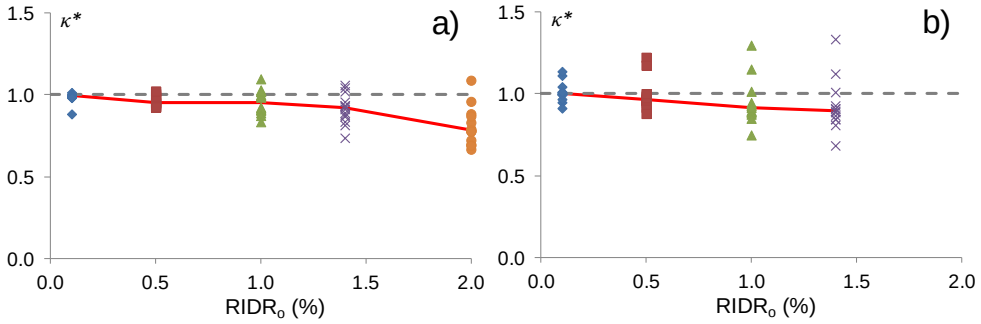

Figure 17. Modified residual capacity index computed from the NF-NF seismic sequences (positive polarity) for both models considered in this study: a) model M1; b) model M2.

As previously discussed, the aftershock capacity associated to demolition, $S_{a,D}$, is also an important parameter to evaluate for the aftershock seismic assessment. Fig. 18 shows a comparison of the $S_{a,A}$ and the $S_{a,D}$ obtained from the M2 model for each individual aftershock (in bars), while the median $S_{a,A}$ and the $S_{a,D}$ is also shown in horizontal red and black dashed lines. It can clearly be observed that for some aftershocks $S_{a,D}$ is smaller, and for some cases significantly smaller, than the $S_{a,A}$. Unlike median $S_{a,A}$, median $S_{a,D}$ decreases in a linear fashion as $RIDR_o$ increases. Similar trend was found for the case of aftershocks with negative polarity. Therefore, it is believed that the aftershock capacity associated to demolition is an important parameter to be quantified during the aftershock seismic assessment of existing structures.

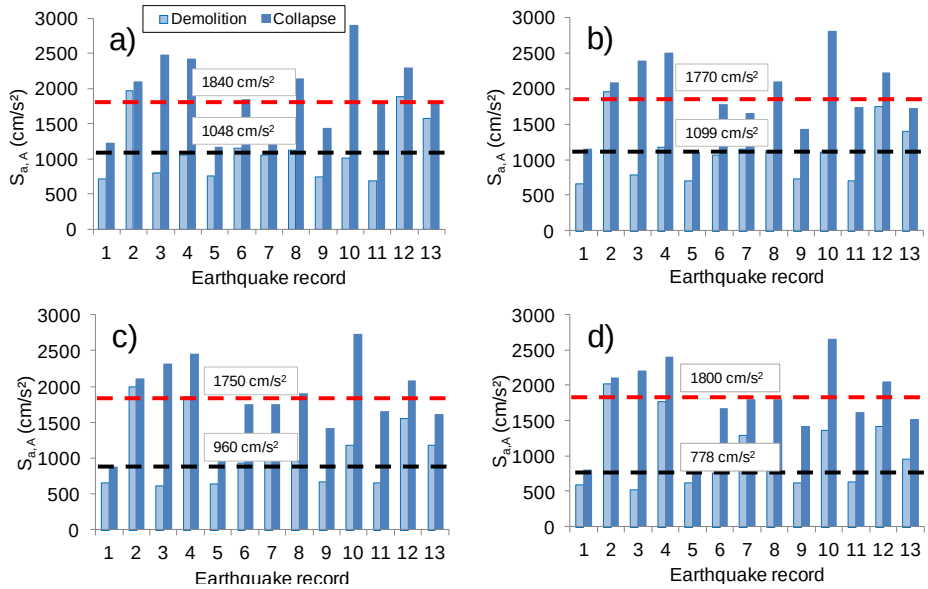

Figure 18. Comparison of $S_{a,A}$ and $S_{a,D}$ corresponding to different $RIDR_o$ for model M2: a) 0.1%; b) 0.5%, c) 1.0%, d) 1.4%.

CONCLUSIONS

Results of this investigation showed that under some seismic sequences, the aftershock collapse capacity decreases as the post-mainshock residual interstory drift, $RIDR_o$, increases. However, it was noted that the building models could experience a re-centering behavior, which lead to an increment in the aftershock collapse capacity as $RIDR_o$ increases. Furthermore, under some seismic sequences, the aftershock collapse capacity was greater than the mainshock collapse capacity. Median values of κ indicate that the modeling approach has significant impact in its trend. Slightly smaller values are found when additional source of stiffness and strength (i.e., interior gravity frames, slab participation) are included in the building model. The median values of κ^* (defined as the ratio of the aftershock

collapse capacity for a given level of $RIDR_o$ with respect to the aftershock collapse capacity computed from $RIDR_o$=0%) also decreases as $RIDR_o$, but the trend depended on the modeling approach.

Particularly, it was highlighted that the aftershock capacity associated to demolition (i.e., associated to a 2% residual interstory drift) is lower than that of the aftershock collapse capacity. This capacity decreases as the level of post-mainshock residual drift increases. Since a building has to be demolished when it reaches a threshold residual interstory drift (e.g., 2%), the aftershock capacity associated to demolition seems a better parameter to measure the residual capacity of buildings subjected to aftershocks.

ACKNOWLEDGEMENTS

The authors express their gratitude to the *Consejo Nacional de Ciencia y Tecnología* (CONACYT) and the *Universidad Michoacana de San Nicolás de Hidalgo* in Mexico for funding the research reported in this paper.

REFERENCES

Applied Technology Council (ATC) (2010) Modeling and acceptance criteria for seismic design and analysis of tall buildings, ATC 72-1, Redwood City, CA, USA

Federal Emergency Management Agency (FEMA) (2012) Seismic performance assessment of buildings. Report FEMA P-58 Vol. 1-Methodology, Washington, DC

Iwata Y, Sugimoto H, Kuguamura H (2006) "Reparability limit of steel structural buildings based on the actual data of the Hyogoken-Nanbu earthquake," *Proceedings of the 38th Joint Panel. Wind and Seismic effects*. NIST Special Publication 1057. pp 23-32

Lignos D (2008) Sidesway collapse of deteriorating structural systems under seismic excitations, PhD. Thesis, Stanford University, EUA

Lignos D, Krawinkler H. (2011a) "Deterioration modeling of steel components in support of collapse prediction of steel moment frames under earthquake loading," *Journal of Structural Engineering*, 137(11):1291–1302

Lignos D, Krawinkler H (2011b) "Prediction and validation of sidesway collapse of two scale models of a 4-story steel moment frame," *Earthquake Engineering and Structural Dynamics*, 40:807–825

Luco N, Bazzurro P, Cornell CA (2004) "Dynamic versus static computation of the residual capacity of a mainshock-damaged building to withstand an aftershock," *Proceedings of the 13th World Conference on Earthquake Engineering*, Vancouver, Canada. Paper no. 2405

Luco et al . (2011) "A methodology for post-mainshock probabilistic assessment of building collapse risk," *Proceedings of the Nineth Pacific Conference on Earthquake Engineering*, Paper No. 210, Auckland, New Zealand

McCormick J, Aburano H, Ikenaga M, Nakashima, M. (2008) "Permissible residual deformation levels for building structures considering both safety and human elements," *Proceedings of the 14th World Conference on Earthquake Engineering*, Beijing, China, Paper No. 05-06-0071

OpenSees. Open System for Earthquake Engineering Simulation - Home Page. <http://opensees.berkeley.edu/> (April 1, 2014)

Psimoulis P, Stiros S (2007) "Measurement of deflections and of oscillation frequencies of engineering structures using robotic theodolites (RTS)," *Engineering Structures*, 29(12): 3312–24

Raghunandan M, Liel AB, Ryu H, Luco N, Uma SR (2012) "Aftershock fragility curves and tagging assessments for a mainshock-damaged building," *Proceedings of the 15th World Conference on Earthquake Engineering*, Lisbon, September, 2012

Ruiz-García J, Negrete-Manriquez JC (2011) "Evaluation of drift demands in existing steel frames under as-recorded far-field and near-fault mainshock–aftershock seismic sequences," *Engineering Structures*; 33: 621–634

Ryu H, Luco N, Uma SR, Liel AB. (2011) "Developing fragilities for mainshock-damaged structures through incremental dynamic analysis," *Proceedings of the Nineth Pacific Conference on Earthquake Engineering*, Paper No. 225, Auckland, New Zealand

Zareian F, Medina RA (2009) "A practical method for proper modeling of structural damping in inelastic plane structural systems," *Computers & Struct*, 88: 45-53